Lithium ion sources for investigations of fast ion transport in magnetized plasmas

Y. Zhang,[a] H. Boehmer, W. W. Heidbrink, and R. McWilliams
Department of Physics and Astronomy, University of California, Irvine, California 92697

D. Leneman and S. Vincena
Department of Physics and Astronomy, University of California, Los Angeles, California 90095

(Received 3 August 2006; accepted 9 December 2006; published online 10 January 2007)

In order to study the interaction of ions of intermediate energies with plasma fluctuations, two plasma immersible lithium ion sources, based on solid-state thermionic emitters (Li aluminosilicate) were developed. Compared to discharge based ion sources, they are compact, have zero gas load, small energy dispersion, and can be operated at any angle with respect to an ambient magnetic field of up to 4.0 kG. Beam energies range from 400 eV to 2.0 keV with typical beam current densities in the 1 mA/cm^2 range. Because of the low ion mass, beam velocities of 100–300 km/s are in the range of Alfvén speeds in typical helium plasmas in the large plasma device. © *2007 American Institute of Physics.* [DOI: 10.1063/1.2431086]

I. INTRODUCTION

Fast ions (FI) with energies large compared to those of the background plasma ions play a key role in space plasmas as well as in controlled fusion related laboratory plasmas. While instabilities and shocks generate fast ions in astrophysical plasmas, in laboratory experiments fast ions are produced by the ionization of injected neutral beams, by ion cyclotron or lower hybrid heating, and as byproducts of fusion reactions.

The interaction of fast ions with waves is of interest in both fusion laboratory and space plasmas but is challenging to study because of difficulties in diagnosing the fast ion distribution function and the wave fields accurately. The goal of the Fast Ion Program associated with the large plasma device[1] (LAPD) at UCLA is to investigate scientific problems of relevance to magnetic fusion research in a probe-accessible plasma that features dimensionless parameters similar to fusion devices. The LAPD facility is ideal for such investigations. The large plasma size (18 m long, 0.75 m diameter) accommodates large pitch angle fast ion orbits and a wide variety of plasma waves. The plasma reproducibility and the computer interfaced diagnostic system accommodate detailed measurements of both the wave fields and the fast ion response. Issues of interest include the transport of fast ions by drift-wave turbulence and the interaction of fast ions with shear Alfvén waves. For some studies, an intense fast ion source that can drive instabilities is required but, for others, a less intense source that is optimized for fast ion transport measurements is needed. The purpose of this "test particle transport" source is to generate a narrow distribution function in both velocity and configuration spaces so that changes in the fast ion distribution caused by the wave fields are readily detected.

The proposed investigations and the fact that the ion source has to be immersed in the plasma puts severe constraints on the properties of the ion gun. An ideal source for this research should have these features (Table I):

- wide energy range (400–2000 eV) to investigate the energy dependence of the interaction;
- low beam ion mass to be able to match the phase velocity of Alfvén waves in helium plasmas;
- operation at magnetic fields up to 4 kG and at any pitch angle;
- low beam divergence to make the beam observable over large distances;
- small energy dispersion;
- high current density to facilitate diagnostics, but small enough to prevent collective wave excitation (test particle investigation);
- small gas load;
- source operation independent of plasma conditions (density, temperature, etc.);
- small size to minimize the perturbation of the background plasma; and
- no magnetic material.

Initially in this program, a commercial argon ion gun from IonTech, featuring a rf discharge as the ion source, was modified for operation in the LAPD (Ref. 2) and used to investigate classical transport[3] and preliminary turbulent transport measurements.[4] Although fairly reliable in operation, it could not be operated at pitch angles larger than 25° and only at magnetic fields of ~1 kG or less. Furthermore, it has much reduced beam production with helium compared to argon, because the higher ionization potential prevents the formation of a sufficiently high plasma density in the source rf coil.

Alternatives to plasma discharges as charged particle source are the solid-state thermionic emitters. While they are widely used as electron emitters, they are used infrequently

[a]Electronic mail: yzhang5@uci.edu

TABLE I. Overview of fast ion sources employed by the UC Irvine FI group in comparison with the ideal source.

Properties	FI source			
	rf source[a]	0.6 in. emitter Li source	0.25 in. emitter Li source	Ideal source for FI experiments[a]
Source type	Plasma type (argon)	Surface ionization (lithium)	Surface ionization (lithium)	No preference
Power input/type	20–100 W (~18.5 MHz)/ rf power	80–100 W (~11 A)/ dc power	12–22 W (~2.2 A)/ dc power	No preference
Physical size (in.) (Cross sectional)	$\sim 9.5 \times 4.25$ in.^{2}	$\sim 4 \times 3$ in.^{2}	$\sim 1.6 \times 1.3$ in.^{2}	Small to minimize plasma perturbation
Beam extraction	Screen (+50–600 V), accelerator (−100–600 V)	Emitter (500–2000 V), grid (−0–2000 V), second grid (floating)	Emitter (500–2000 V), first grid (−0–2000 V), second grid (floating)	Wide energy range (50–3000 eV)
Modulation type/purpose	Modulate rf power /to prevent source overheating	Modulate extraction biases /to preserve emitter lifetime and increase beam extraction	Modulate extraction biases /to preserve emitter life time and increase beam extraction	No preference
Beam profile	Adjustable, up to 3 cm max diameter	Adjustable, up to 1.5 cm max diameter	Adjustable, up to 0.6 cm max diameter	>0.32 cm diameter (size of a standard probe collector)
Beam current	2.0 mA/cm^2	1.0 mA/cm^2	1.0 mA/cm^2	~1.0 mA/cm^2
Beam energy/spread	<10%	<4%	<4%	<10%
Beam divergence	3°	~3°	~3°	<3°
Pitch angle	0–25°	20–90°	17–90°	0–70°
Ambient magnetic field	<1.0 kG	Up to 4 kG	Up to 4 kG	Up to 4 kG
Consumable	None	0.6 in. Li emitter	0.25 in. Li emitter	Economical
Maintenance	Remove coating on discharge chamber and grids	Replace emitter	Replace emitter	Minimal
Influence on LAPD plasma	Argon neutral leak	Minimal out gassing	Minimal out gassing	Modest to minimize neutral collisions
Influence by LAPD plasma	Neutralizing electrons aid fast ion extraction	Electron saturation current on emitter increases HVPS current load	Electron saturation current on emitter increases HVPS current load	Modest to maintain steady beam output

[a]Reference 2.

as ion sources because of their limited current density. Of particular interest as a thermionic ion emitter for the FI program is lithium aluminosilicate (LAS). The type of aluminosilicate used in this article is beta eucryptite.[5,6] Apart from lithium, these ceramics are also available for other alkali ions: sodium, potassium, and cesium. Because of their ceramic nature, these emitters are inert to atmospheric constituents at room temperature but deteriorate in the presence of oxygen, vacuum oil, etc., at operating conditions (1000–1200 °C).

LAS sources have been used before in plasma related experiments. A small gridded lithium ion source was used to investigate ion drift orbits in the vacuum magnetic field of the Compact Auburn Torsatron.[7] Lithium ion and neutral beam sources, placed externally to the plasma chamber, are also used for optical and beam probe diagnostics in tokamak and stellarator configurations.[8–12] Since these sources are operated in the absence of plasma electrons and system magnetic fields, they can employ a Pierce configuration,[13] which generates low emittance, high current density beams.

This article describes the development of two lithium ion sources of different sizes that can be operated in a high density, magnetized plasma. In Sec. II, the design characteristics of these guns and their performance in an ultrahigh vacuum chamber at UC Irvine are discussed. The LAPD system at UCLA, in which the FI investigations will be performed, is briefly described in Sec. III together with an investigation of lithium ion gun operation in that system. In Sec. IV, potential improvements of the ion sources are discussed.

II. LITHIUM ION SOURCE DESIGN AND CHARACTERIZATION

The Pierce geometry is the ideal configuration for charged particle sources since it has no beam perturbing grid structures. Unfortunately, it cannot be used for the investigations of FI behavior in plasmas because the background plasma constituents streaming into the gun will modify the vacuum electric field of the electrodes. In addition, the external magnetic field will modify the beam orbits within the large physical structure of a Pierce source. Therefore, a gridded gun configuration was chosen in which the emitter–extraction grid separation was small enough to render beam orbit modifications within the gun structure by $v \times B$ and $E \times B$ forces insignificant.

Two lithium ion guns with lithium aluminosilicate as thermionic emitters of different sizes (0.6 and 0.25 in. diameter, Heat Wave Inc.[14]) were designed, constructed, and characterized at UC Irvine. Lithium emitters with typical isotope concentrations of 92.5% Li-7 and 7.5% Li-6 are chosen for testing the FI sources. Li-7 isotopically purified emitters are available for future experiments. The cross section of a generic lithium ion gun is schematically shown in Fig. 1. The actual configurations are scaled to the two different emitter sizes. While the gun with the 0.6 in. emitter is the prototype,

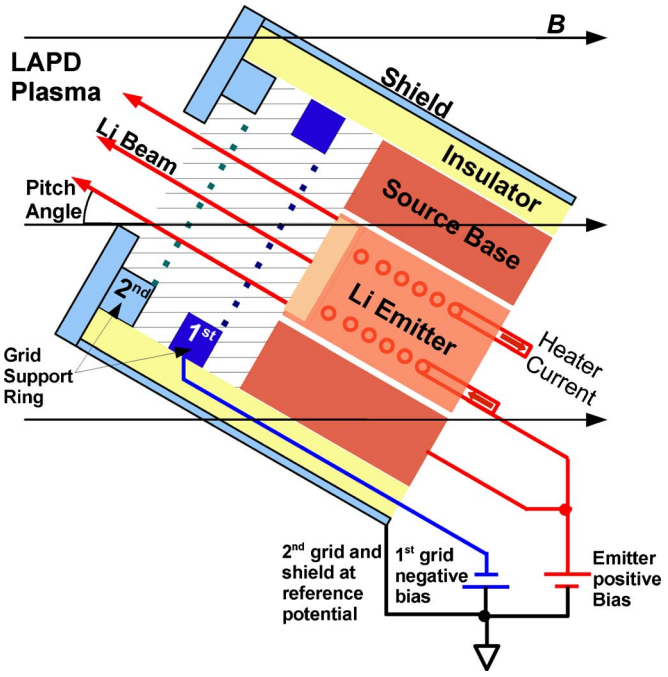

FIG. 1. (Color online) Cross sectional view of a generic lithium ion source in the LAPD plasma at a pitch angle of 30°. Shaded area corresponds to the beam extraction region, which is also the domain used to simulate the field line configuration in Fig. 4.

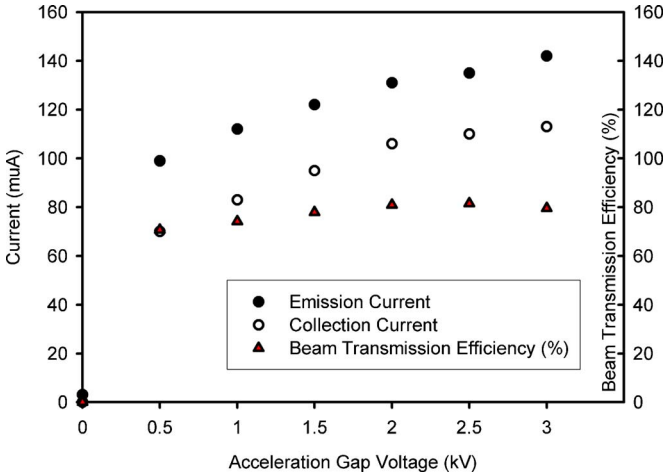

FIG. 2. (Color online) 0.6 in. emitter gun emission and collection current vs acceleration gap voltage. Beam transmission efficiency is calculated for each pair of current levels. (Total grid optical transparency is 81%.)

the smaller gun was developed to decrease the perturbation of the LAPD plasma by the gun housing and to be able to use standard 50 mm diameter vacuum interlock valves of LAPD. Both guns were tested first in an ultrahigh vacuum system at UC Irvine.

Since the ion emission from LAS is not purely a thermally activated process but can be enhanced by an external electric field (Schottky effect), it is desirable to have a high potential difference between the emitter and the first grid. Therefore, to produce sufficient beam currents even at low beam energies, an acceleration-deceleration strategy is employed where the emitter is biased positive (with respect to the gun housing and the second grid) to the desired beam energy while the first grid is biased to an appropriately high negative potential. Measured by a laser beam, the optical transparency of the grid system poses an upper bound for the beam transmission efficiency (collection current/emission current). Strong field line distortions or space charge effect will cause the beam transmission efficiency to decrease from the optical transparency.

The ion guns are first tested at UC Irvine in an ultrahigh vacuum chamber, usually without the presence of a plasma to neutralize the beam space charge. The distances from emitter to exit are 1.88 cm for 0.6 in. emitter source and 1.45 cm for 0.25 in. emitter source. During vacuum operations, it was observed that the collector and the probe have to be within a few centimeters from the source exit to measure the beam current. To test the basic performance of the ion guns, the emission current was monitored as a function of emitter temperature as measured by an optical pyrometer viewing the emitter through a quartz vacuum window. The emissivity of the emitter surface, assuming $\varepsilon=0.8$, could cause ~65 °C of temperature underestimation. In this work, the emitter temperature is recorded without emissivity corrections and serves as a relative indicator of beam current performance. For the 0.6 in. emitter at 1150 °C and biased to 2 kV, the observed current is 2 mA which corresponds to a current density of 1 mA/cm^2. The secondary electron emission from the first grid is measured to be less than 1% of emission current, which causes less than 10% of ion transmission overestimation. With two 40 lines/in., 91% transmission Molybdenum grids, the optical transparency is 81%. Figure 2 compares the emission current and the current to an outside collector (2.5 cm from the emitter) as a function of extraction voltage with the emitter temperature at 1050 °C. The space charge limit at 1000 V of extraction voltage is ~200 μA, which indicates that most of the current levels are limited by thermionic emission instead of space charge effect. On average, nearly 80% of the ion beam is transmitted through the grid holes with the acceleration voltage above 500 V. Positioning the gun axis at an angle of 45° with respect to an external magnetic field of up to 4 kG did not result in a change of emission current. Figure 3(a) shows the beam cross section 5 cm outside the gun in the UC Irvine chamber, using a 3 mm diameter disk collector, demonstrating a good beam optics. It should be noted that, in Fig. 3, the emitter current was intentionally kept low at (a) ~0.1 mA and (b) ~10 μA to reduce the radial space charge modification of the beam profile. In Fig. 3(b), the beam radial profile is still widened by ~10% from the radial expansion.

Distortion of the ion orbits within the gun structure can be caused by the fringing fields at the edge of the emitter and the grid support rings as well as by equipotential surface deviations from being strictly parallel in close vicinity of the grid wires. These effects are more prevalent for the small diameter emitter. Furthermore, care must be taken in placing insulating structures in such a way that accumulated charges will not distort the field. To visualize the electric field pattern within the actual gun structures, the FEMLAB software (COMSOL, Inc.) is used to calculate the 2D equipotential lines in cylindrical coordinates and estimate the space charge effect [Fig. 4(a)–4(c)]. The models' boundary conditions are set at typical operating conditions. Since FEMLAB lacks a

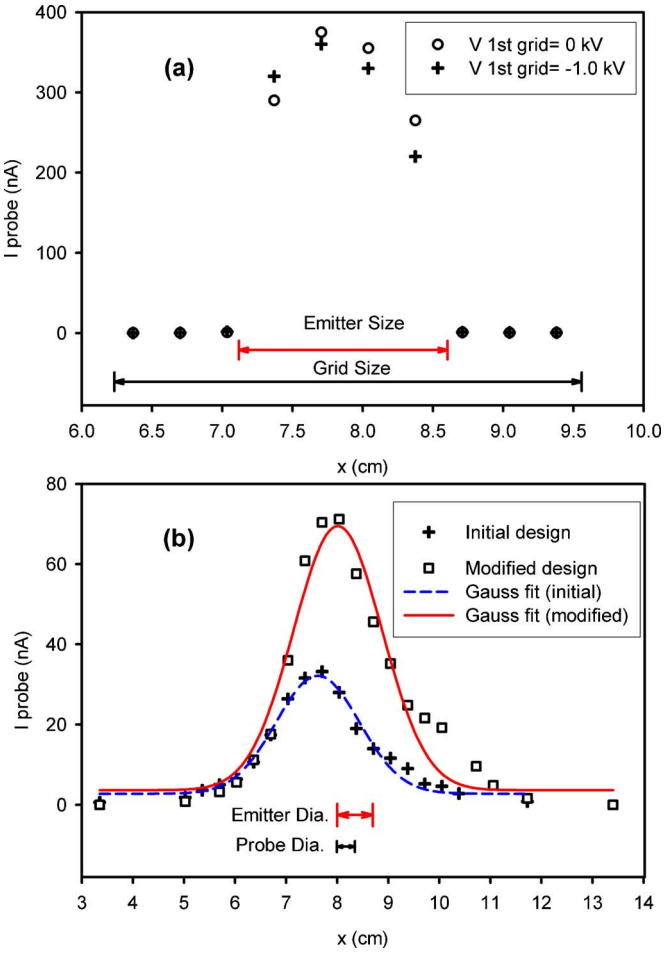

FIG. 3. (Color online) (a) 0.6 in. emitter gun beam profile across beam center collected 5 cm away from the beam exit. Profiles are taken with +2.0 kV emitter bias and 1050 °C emitter temperature. (b) Comparison of 0.25 in. emitter gun beam profiles before and after modifying first grid structure. Profiles are taken with +600 V emitter bias, −100 V first grid bias, and 1050 °C emitter temperature.

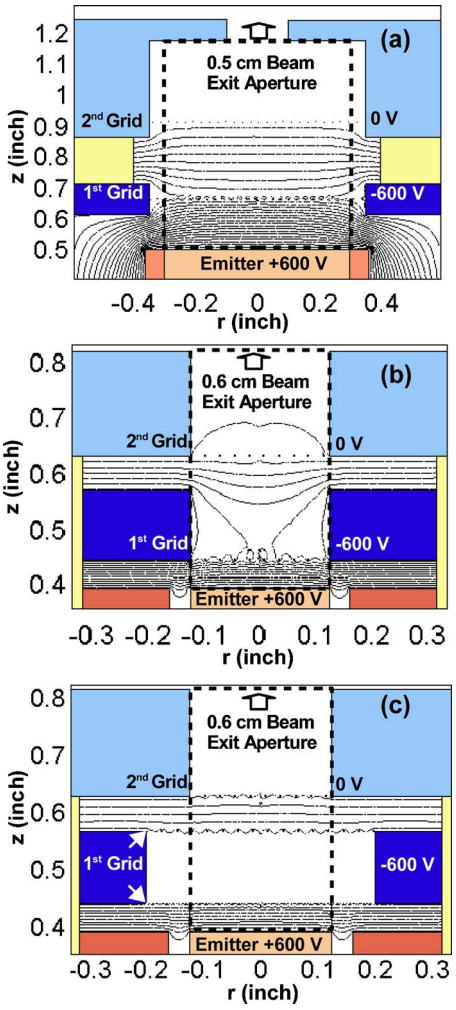

FIG. 4. (Color online) Electrostatic potential lines calculated according to different gun configurations: (a) 0.6 in. emitter gun, (b) 0.25 in. emitter gun initial design with a single first grid next to the emitter, and (c) 0.25 in. emitter gun modified design with two first grids biased negatively. Cylindrical symmetry is assumed in simulations and all grid sizes are to scale (may appear to be a single dot). Dashed boxes show where space charge is uniformly distributed along the beam paths. Simulations are powered by FEMLAB (COMSOL, Inc.).

Poisson solver, the space charge effect of the beam is estimated by imposing uniformly distributed space charge along the beam path. A 0.1 mA/cm^2, Li ion beam at 600 eV energy corresponds to a reference charge density of $\rho_0(7.23\times10^{-6}\ C/m^3)$. A potential barrier comparable to the beam energy does not appear in the source until the imposed charge density is increased to $100\rho_0$. It can be seen that for the 0.6 in. emitter gun [Fig. 4(a)] the fringing fields and the field distortions around the grid wires are minimal. Since this ion gun is usually operated with a 0.5 cm aperture, sampling only the center part of the beam, it produces a high quality beam (see Sec. III). In contrast, the 0.25 in. emitter gun, where, to reduce edge effects, the emitter-grid spacing was reduced from 2.50 to 1.25 mm, these effects are more severe. Figure 4(b) shows the field pattern for the 0.25 in. emitter gun initial design using a 40 lines/in. first grid. Because the grid is much closer to the emitter, the equipotential lines are greatly distorted around the grid wires, compared to Fig. 4(a) where the same grid size but a larger spacing was used. In addition, in the deceleration stage, the fringing field in the grid support ring reaches the center of the beam. As a result of both effects, the radial beam profile for this gun is wider than the emitter diameter [Fig. 3(b)] and the transmitted beam current is greatly reduced (~30% of emission current). To improve the beam quality, a 90 lines/in. first grid was installed and an additional 40 lines/in. grid was installed on the opposite side of the grid support ring with a wider aperture [0.40 in. inside diameter]. The improvement of the field pattern is evident from Fig. 4(c). Although the radial distribution of the beam [Fig. 3(b)] is similar, the transmitted beam current doubles with the modified design, in spite of the total optical transparency drop from 81% to 64%. The beam transmission efficiency is also improved to ~49%–66% (uncertainty caused by possible secondary electron emission) that is comparable to the optical transparency.

A large diameter planar collector that measures the total emitted beam current was used to acquire the energy distribution of the beam by taking the derivative of the collected current with respect to the collector bias. Figure 5 gives examples of the beam energy distributions for the 0.25 in. emit-

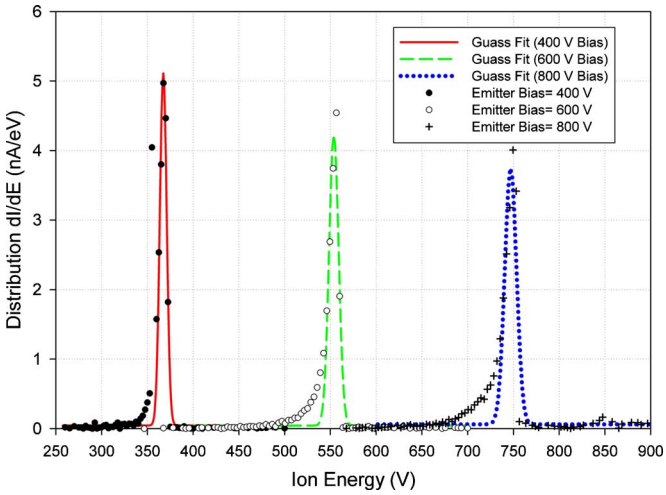

FIG. 5. (Color online) Energy distributions from 0.25 in. emitter gun with different emitter biases. Data taken with −100 V first grid bias and 1100 °C emitter temperature.

ter gun. The width is about 4% of the beam energy without deconvolving the energy resolution of the collector.[15] For these LAS emitters, the actual energy spread of a near zero energy beam is given by a Maxwellian distribution determined by emitter temperature, which is about 0.25 eV. The low energy tail of the distributions, which becomes more prominent with increasing beam extraction voltage, is likely due to the field line deviations from directions perpendicular to the emitter, e.g., those around the wires of the extraction grids, as well as the increased resolution width of the collector at higher beam energy.

From these results, it is evident that great care has to be taken in the design of gridded guns for good performance and that the equipotential surfaces in the acceleration and deceleration stages of the gun should deviate from planes as little as possible since these field errors influence both the energy spread and the divergence of the beams. Edge effects can be minimized by extending the parallel planes defined by emitter and first grid to larger radii. In the acceleration stage, this is accomplished by providing a shield structure around the emitter and by the grid support ring. In the deceleration stage, again to provide flat equipotential planes, extra grids are sometimes necessary even though they decrease the total optical transparency.

With a specially fabricated integral power supply for high voltages and heater current, the ion guns can be operated either in the dc mode or pulsed at the 1 Hz repetition rate of the LAPD plasma using a minimum of 15 ms pulse length. From the experience of operating the larger gun at LAPD, the emitter lifetime was found to be about 20 h for an average beam current density of 1 mA/cm^2. In a high vacuum environment, the lifetime is considerably longer according to Heat Wave Labs, Inc.

III. LITHIUM GUN PERFORMANCE IN A HIGH DENSITY, MAGNETIZED PLASMA

In LAPD, the magnetically confined, linear plasma is generated by applying a 50–100 V voltage pulse between a 75 cm diameter barium oxide cathode and a grid anode with

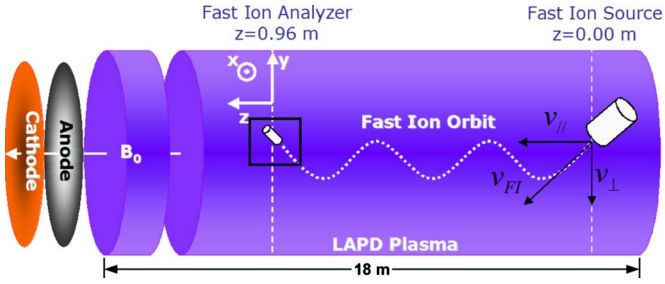

FIG. 6. (Color online) Fast ion experiment configuration in the LAPD plasma (schematic). Figure shows that FI completes three cyclotron orbits before being collected by the fast ion analyzer three ports away from the source (0.96 m). The analyzer scans in *x-y* plane for beam spatial profile. The details of FI diagnostics inside the box will be shown in Fig. 7.

a 2 kA discharging current pulse at a 1 Hz repetition rate. Operating gases include hydrogen, helium, argon, and neon. During the discharge of ~8 ms duration, the plasma density can reach 5×10^{12} cm^{-3} with an electron temperature of 10 eV. The plasma density decays in the afterglow with an initial time constant of ~10 ms and plasma temperature of ~100 μs. While the plasma contains various modes of turbulence during the discharge, it is quiet in the afterglow. The planned FI investigations of plasma turbulence will primarily focus on FI interactions with waves and turbulence during the high density discharge, when the lithium beam density of 5.0×10^{8} cm^{-3} is typically four orders of magnitude smaller than the plasma density during the discharge. Plasma parameters and fluctuations are diagnosed with a millimeter wave interferometer, Langmuir probes of various configurations, and three axis dB/dt loop probes for the measurement of magnetic field fluctuations, for example, of Alfvén waves.

Supported by stainless steel tubes that also carry the heater and high voltage cables, the ion guns are placed into the LAPD vacuum chamber at various points along the axis of the system. Pumped chevron seals allow the radial motion and rotation of the guns without vacuum leaks. The ion gun and power supply system can be separated electrically from the vacuum chamber ground. This allows the ion gun to float at the plasma potential, decreasing the perturbation of the plasma by the ion gun housing. The plasma–ion gun configuration at LAPD is shown schematically in Fig. 6.

The operation of these ion guns inside a plasma environment has pros and cons compared to operation in a vacuum field chamber. In the LAPD plasma, the beam with the maximum current output is charge neutralized by the plasma electrons since the plasma charge density, even during the afterglow, exceeds that of the beam by three orders of magnitude, which is an obvious benefit for the fast ion beam orbit studies. There are also issues to be aware of when the source is immersed in a plasma. Firstly, since the ion sources are often floated to reduce plasma perturbation, the exiting FI energy is referenced to plasma floating potential, which is subject to change of plasma conditions. For example, the floating potential in the discharge is ~10 V higher than that in the afterglow, which causes ~10 eV of difference in beam energy given identical extraction grid biases. Secondly, because the emitter is at the positive beam voltage and because the grid holes, for any useful plasma density, are large compared

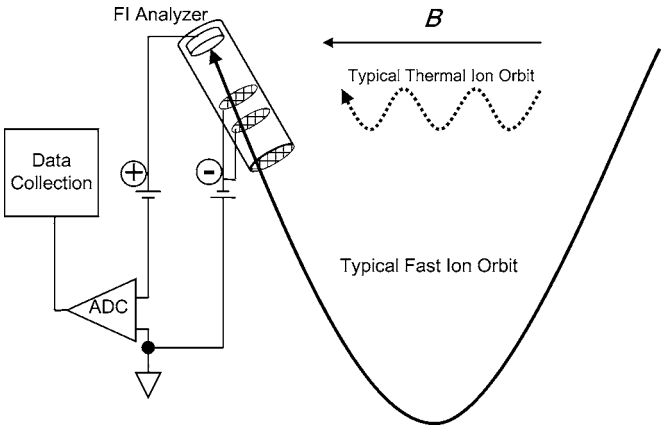

FIG. 7. Illustration of the fast ion analyzer that distinguishes fast ion signals from thermal particles.

to the Debye length, plasma electrons can reach the emitter electrode of the ion gun. For operation in the afterglow phase of the LAPD plasma, this just adds a few milliamperes to the load of the high voltage power supply but otherwise does not impair the function of the ion gun. On the other hand, during the high density discharge, this current becomes excessively large. In this case, the ion gun must be positioned at a sufficiently large pitch angle so that the plasma electrons, tied to the magnetic field lines, are prevented from reaching the emitter. This is schematically indicated in Fig. 1.

Because the 0.6 in. diameter beam of the larger ion gun is more than sufficient for this FI transport investigation, to achieve a better spatial resolution, this gun was operated either with a 2 mm wide rectangular or a 5 mm diameter circular aperture.

Several probe designs to determine the position and energy distribution of the ion beam in the LAPD plasma were tested. To have good spatial resolution as well as sufficient collecting area, the probe collector has a diameter of typically 3.2 mm. With a beam current density considerably less than 1 mA/cm^2 typical probe current signals are in the $0.1-1$ μA range at large distances from the ion gun. Detection of these small signals at the LAPD, particularly during the discharge, is challenging. The kiloampere level plasma discharge current pulse causes stray signals due to ground loops and capacitive as well as inductive coupling, which have to be eliminated by proper grounding and shielding. More important is the influx of background plasma ions and electrons into the detector/analyzer. FI analyzers taking advantage of either electrical or geometrical[16] shielding have been developed but none of them can detect FI signals during the discharge. The best design combines both shielding techniques together to detect FI signal successfully in the discharge (Fig. 7).

The collector of the FI analyzer is biased positively at various voltages to obtain the energy distribution of the ion beam in the LAPD plasma. For a 600 eV beam with a pitch angle of 28°, measured 1 in. away from the beam exit in the LAPD afterglow plasma, the energy spread (3%) is similar to that measured in a vacuum magnetic field. A continuous low energy tail is observed in the distribution. Further discussions of energy distribution measurements at different plasma and beam conditions will be included in a separate paper.

For small pitch angles ($<15°$), the collector of the FI analyzer is biased sufficiently positive ($\sim+50$ V) to reject plasma ions. Since this would result in the collection of plasma electrons, an intermediate grid is biased negative (~-50 V). In the discharge plasma, the Debye length (~15 μm) is smaller than the grid holes (~70 μm) that become partially transparent for electrons. Since grids with sufficiently small holes are not practical, two successive grids on the same potential were employed, the first grid reducing the plasma density and therefore increasing the Debye length for the second grid to become effective. For larger pitch angle ($>15°$) beams, the tubular housing surrounding the recessed collector is directed parallel to the local ion beam trajectory. The collector is recessed in the housing by more than the plasma electron and ion Larmor radii (Fig. 7) to shield the collector from thermal particles geometrically. Thus one of the advantages of choosing a large pitch angle ($>15°$) beam for this research is obvious: both electrical and geometrical shielding can work together to maximize the FI signal to noise ratio.

Figure 8 shows signal traces of a typical large pitch angle beam diagnostics. They are, as in four separate plots, the temporal evolution of the LAPD plasma line density, the voltage pulse applied to the emitter, and the emitter current and the probe current for gun operation in the afterglow and during the discharge. The afterglow and the discharge traces are scanned independently but presented here together according to their timings relative to the LAPD plasma discharge. Both time windows, (1) and (2) in the figure, start from 20 ms after each emitter bias trigger and last for 6 ms, during which time the plasma conditions and ion gun performance are steady. The gun is operated at an angle of 28° with respect to a 1.5 kG magnetic field. The beam signals are measured one port from the gun (32 cm) where the ion beam has performed one cyclotron orbit. The probe signal carries some residual fluctuations due to the plasma pulse especially in the discharge, but the net signal is clearly revealed after subtracting the beam-off signal from the beam-on signal.

Measurements of the beam profile in the LAPD plasma are shown in Fig. 9 where the FI analyzer is scanned in the x-y plane (Fig. 6) with spatial steps of 1.0 mm in x and 2.0 mm in y. In all cases, the 0.6 in. emitter ion gun is operated with a 5 mm aperture. Figure 9(a) displays the transverse beam profile for a zero pitch angle beam in the afterglow plasma, 2.5 cm from the ion gun. Figure 9(b) is a beam contour taken during the afterglow plasma [time window (2) in Fig. 8]. It was found in our previous FI beam investigations[2] with argon ions that, for helical beams, the slightly divergent beam emanating from the gun is refocused at integer numbers of gyro orbits. Therefore, orbits are always selected to complete integer numbers of gyro orbits that coincide with the location of diagnostic ports. In Fig. 9(b) the beam has completed approximately one gyro orbit before reaching the analyzer at one port away (32 cm) along the z direction. The beam spot is elongated in the direction of gyro motion. A likely explanation for this effect is

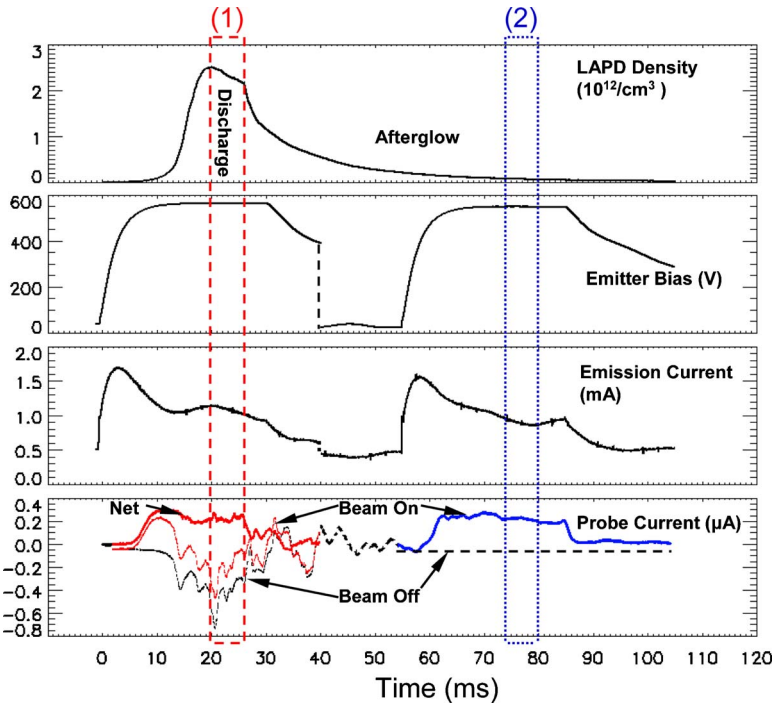

FIG. 8. (Color online) Typical fast ion analyzer collected signal with reference to LAPD plasma density and lithium source properties (0.6 in. emitter gun). Conditions: $B=1.5$ kG; peak emitter bias=554 V; first grid bias=−100 V; analyzer axial distance from source=32 cm; analyzer grid biases are +50 V and −50 V. Two different time windows: (1) Discharge (averaging every 15 shots and every 128 continuous samples; sample rate at 50 MHz; 6 ms duration). Beam-on (red-dashed) signal is compared to beam off (dashed). Net signal is shown as beam on minus beam off. (2) Afterglow (averaging every three shots and every 128 continuous samples; sample rate at 25 MHz; 6 ms duration). Beam-on (blue) signal is compared to beam off (dashed).

that, due to a finite energy spread, ions with different axial velocities take different amounts of time to reach the z position of the detector. The gyro phase φ at the detector is $\omega\Delta z/v\cos\theta$, where ω is the cyclotron frequency, Δz is the FI traveled distance in the z direction, v is the FI speed, and θ is the FI pitch angle. Since ω is independent of energy, ions with different energies reach the detector with different gyro phases. The variation in gyro phase with energy $\Delta\varphi$ can be expressed as

$$\Delta\varphi = \sqrt{\frac{m_{\mathrm{Li}^+}}{8E^3}}\frac{\omega\Delta z}{\cos\theta}\Delta E, \tag{1}$$

where m_{Li^+} is the mass of lithium FI and ΔE is the variation of FI energy. For a 20 eV beam energy spread, using parameters in Figs. 8 and 9(b), the variation is 6.5° in gyro phase and 0.31 cm in beam width along the gyro orbit. In contrast, the radial beam width is determined primarily by the emitted radius of the beam.

The curvature of the gyro orbit at the beam collection point causes a small portion of the beam to be absorbed on the probe wall before reaching the recessed collector, which is the vignetting effect discussed in Ref. 16. Since the analyzer is always rotated in the y-z plane to match the incoming beam, the collector effective aperture in the y direction is close to the collector diameter of 3.2 mm. The collector effective aperture in the x direction is determined to be ~2.7 mm by a simulation of an ensemble of FI orbits in the analyzer geometry in the x-z plane. If a perfect 5 mm diameter beam is collected in this manner, the widths of the beam along the x and y directions, convoluted with the collector effective aperture, are 5.7 and 5.9 mm, respectively.

To analyze the radial beam profile, the white dash curve is first fitted in Fig. 9(b) to indicate the beam trajectory in the x-y plane with a radius of 2.7 cm that is calculated from the beam launching conditions. Then the profile data are extracted along radial lines and fitted to Gaussian distributions with the goodness of fitting (χ^2) recorded as statistical weights.[3] An example of a radial line is shown in Fig. 9(b) connecting the cross hair and the orbit center.

Radial profiles of the beam are shown in Fig. 10 for the discharge and the afterglow signals. Both profiles are weighted averages of all the available radial lines with sufficient signal intensity. The profiles are accurately represented by Gaussian distributions. The error bars correspond to temporal fluctuations of beam local intensity, and they are calculated by taking standard deviations (STD) of 60 continuous time bins (0.1 ms) of beam intensity at each radial location. The discharge beam signal is noisier than the afterglow signal. The full width at half maximum (FWHM) for each curve is close to the expected beam collection width.

IV. SUMMARY AND FUTURE WORK

Lithium ion sources using lithium aluminosilicate as a thermionic emitter were developed and characterized. Two commercially available emitter sizes (0.6 and 0.25 in.) with integrated heater assembly were used. A compact ion gun structure was chosen featuring grids for acceleration-deceleration sections. In principle, the ion guns can be operated at any angle with respect to the magnetic field; although, at high plasma densities, a minimum pitch angle must be used to avoid plasma electron loading of the emitter circuit. Typical ion beam densities are in the 1 mA/cm^2 range at beam voltages between 400 and 2000 V. The ion guns successfully operated in the high plasma density environment of the LAPD.

These sources are well suited for fast ion physics studies. In a preliminary study,[4] 600 eV lithium ions interacted with shear Alfvén waves at the Doppler-shifted cyclotron

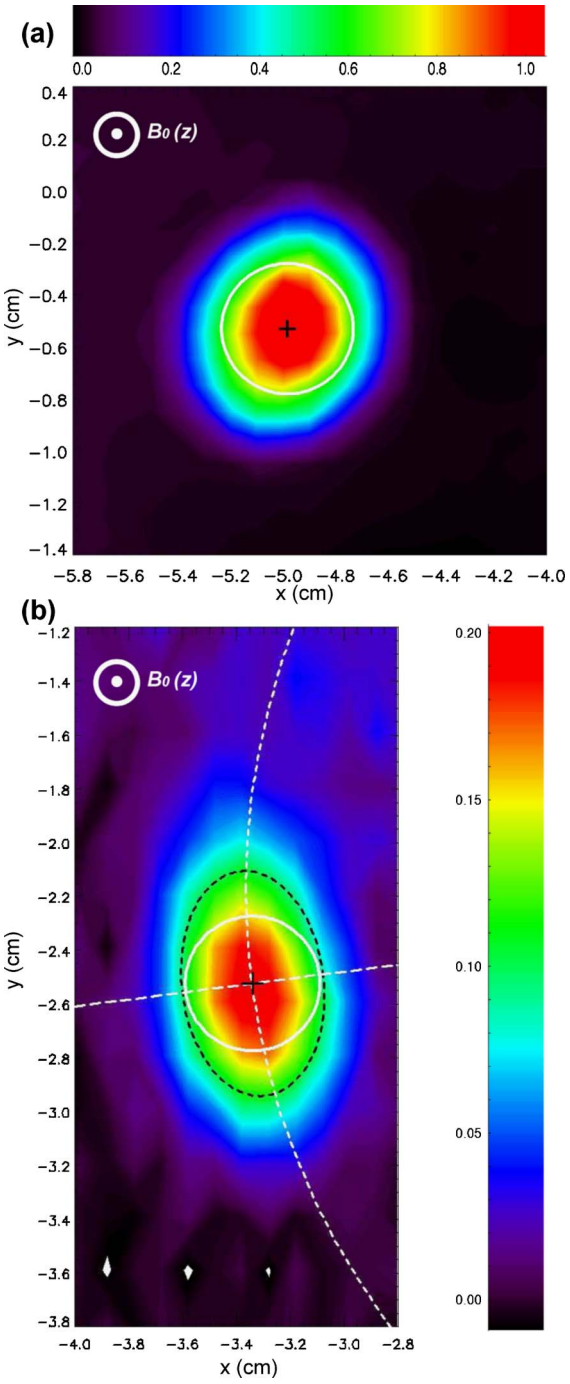

FIG. 9. (Color online) Contours of 0.6 in. emitter gun beam profile in the LAPD plasma (color bars in μA; origin at LAPD machine center). White solid circle: 0.5 cm diameter aperture (ideal beam spot); black cross hair: beam center; black dash ellipse: ellipse with semimajor and semiminor axes calculated from two-dimensional (2D) Gaussian fit of beam contour; white dash curve: part of the beam orbit projection of x-y plane with theoretical radius of 2.73 cm; white long dash line: radial line connecting beam center and orbit center.

resonance. Other planned studies include measurements of the acceleration of fast ions by fast waves at harmonics of the cyclotron frequency and measurements of fast ion diffusion caused by drift-wave turbulence.

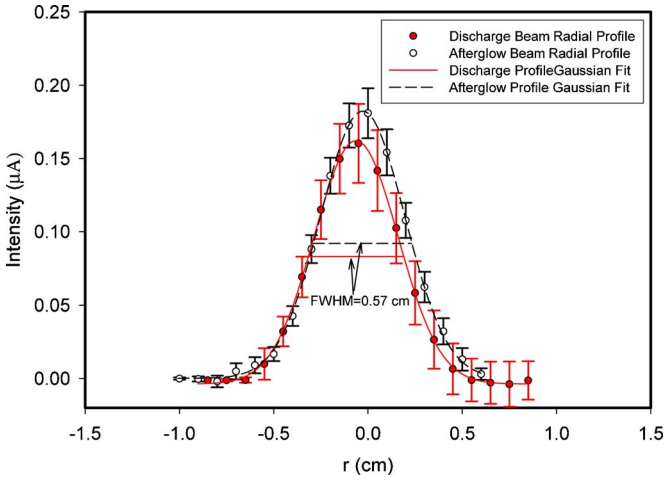

FIG. 10. Weighted average radial beam profile in the discharge and the afterglow. $r=2.7$ cm corresponds to the predicted center of the gyro orbit. The horizontal line indicates the FWHM for each curve.

In terms of our design criteria (Table I), the only significant disadvantage of these sources is their finite life. In the LAPD environment, the emitters have a lifetime of ~20 h compared to the manufacturer's quoted lifetime of 200 h.[17] The reason for this limited lifetime requires further investigation.

ACKNOWLEDGMENTS

The authors gratefully acknowledge the assistance by W. Gekelman, T. Carter, and B. Brugman. An important part of this work was performed at the LAPD basic plasma user facility supported by NSF/DOE.

[1] W. Gekelman, H. Pfister, Z. Lucky, J. Bamber, D. Leneman, and J. Maggs, Rev. Sci. Instrum. **62**, 2875 (1991).
[2] H. Boehmer, D. Edrich, W. W. Heidbrink, R. McWilliams, and L. Zhao, Rev. Sci. Instrum. **75**, 1013 (2004).
[3] L. Zhao, W. W. Heidbrink, H. Boehmer, and R. McWilliams, Phys. Plasmas **12**, 052108 (2005).
[4] Y. Zhang *et al.*, Bull. Am. Phys. Soc. **FP1**, 00075 (2005).
[5] M. Sasao*et al.*, IEEE Trans. Plasma Sci. **33**, 1872 (2005).
[6] J. P. Blewett and J. Jones, Phys. Rev. **50**, 464 (1936).
[7] G. E. Sasser, S. F. Knowlton, R. F. Gandy, H. Lin, E. E. Thomas, and M. A. Owens, Rev. Sci. Instrum. **66**, 324 (1995).
[8] D. C. Pritchard, R. F. Gandy, J. D. Hanson, S. F. Knowlton, H. Lin, G. E. Sasser, E. Thomas, Jr., and J. Cooney, Phys. Plasmas **4**, 162 (1997).
[9] D. M. Thomas *et al.*, Rev. Sci. Instrum. **72**, 1023 (2001).
[10] R. J. Fonck, P. A. Duperrex, and S. F. Paul, Rev. Sci. Instrum. **61**, 3487 (1990).
[11] G. McKee *et al.*, Rev. Sci. Instrum. **70**, 913 (1999).
[12] D. M. Thomas, Rev. Sci. Instrum. **66**, 806 (1995).
[13] A. T. Forrester, *Large Ion Beams—Fundamentals of Generation and Propagation* (Wiley, New York, 1988).
[14] Heat Wave Labs, Inc., alkali ion source document, http://www.cathode.com/pdf/tb-118.pdf
[15] H. B. Haskell, O. Heinz, and D. C. Lorents, Rev. Sci. Instrum. **37**, 607 (1966).
[16] W. W. Heidbrink and J. D. Strachan, Rev. Sci. Instrum. **56**, 501 (1985).
[17] O. Heinz and R. T. Reaves, Rev. Sci. Instrum. **39**, 1229 (1968).